Metal−Oxide Interfacial Reactions: Encapsulation of Pd on TiO_2 (110)

Qiang Fu, Thomas Wagner,* Sven Olliges, and Heinz-Dieter Carstanjen

Max-Planck-Institut für Metallforschung, Heisenbergstrasse 3, D-70569 Stuttgart, Germany

Received: August 30, 2004; In Final Form: October 14, 2004

The model system Pd/TiO_2 (110) was used to evaluate the correlation between metal encapsulation and electronic structure of TiO_2 crystals. We observed encapsulation of Pd clusters supported on TiO_2 crystals, which were heavily Ar^+ sputtered, Nb-doped, or reduced by vacuum annealing. In contrast, encapsulation was not observed on unreduced, undoped, or slightly sputtered TiO_2 crystals. Our results indicate a strong dependence of the encapsulation process on the electron density in the conduction band of TiO_2 and on the space charge formed at Pd/TiO_2 interfaces. This behavior is controlled by the initial position of the Fermi energy level (E_F) of the metal and the oxide before contact is established. We proved that encapsulation reactions are favored by n-type doping of the oxide and a large work function of the metal. On the basis of this mechanism, we conclude on general trends controlling encapsulation reactions of oxide-supported metal clusters and the strong metal−support interaction (SMSI).

1. Introduction

The interactions between metals and oxide supports, so-called metal−support interactions, are of great importance in heterogeneous catalysis.[1] Specifically, the strong metal−support interaction (SMSI) was first termed by Tauster et al.[2] to explain the suppression of the H_2 and CO chemisorption capacity of metal clusters on TiO_2 chemically reduced at high temperatures. Later, the term SMSI was used more generally to account for changes in catalytic activity and selectivity when group VIII metals, supported on reducible oxides (e.g., TiO_2, CeO_2, V_2O_5), were treated by high-temperature reduction (HTR) processes.[3,4] Two major factors contribute to the SMSI states, so-called electronic and geometric factors.[1−4] The electronic factor is determined by a perturbation of the electronic structure of the metal catalyst. This perturbation originates from an interaction between the cluster and the oxide support, for example, a charge transfer between the metal and the oxide.[5,6] The geometric factor is due to a physical covering of metal particles by a thin layer of reduced oxide support (encapsulation or decoration model), blocking active catalytic sites at metal surfaces. A variety of experiments have confirmed encapsulation reactions for different metal/oxide systems:[4,7−18] Bernal et al.[7,8] showed via high-resolution transmission electron microscopy (HRTEM) investigations that the major structural feature of high-temperature reduced Rh/TiO_2 and Rh/CeO_2 catalysis systems is the formation of oxide layers on top of the metal clusters. Diebold and co-workers[9] succeeded in recording atomically resolved surface images of encapsulated Pt clusters on TiO_2 (110). These authors proposed an oxygen terminated $TiO_{1.1}$ (111) double layer to be the covering layer on Pt. Bowker and co-workers[10,11] reported a similar well-ordered titania layer with the structure of TiO or $TiO_{1.4}$ decorating Pd clusters after high-temperature treatment. Frequently, various surface spectroscopic methods, such as X-ray photoelectron spectroscopy (XPS), Auger electron spectroscopy (AES), and low energy ion scattering spectroscopy (LEIS), are applied to study encapsulation phenomena. The detection of partially reduced oxides was considered to be a proof for encapsulation reactions in the following systems: Pd/TiO_2,[10] Pt/TiO_2,[12,13] and Rh/TiO_2.[14−16] In these studies, the detection of a partial reduction of metal ions (e.g., Ti^{n+} ($n < 4$)) was attributed to the formation of a reduced oxide layer on top of the metal clusters.

From previous experiments, it is well accepted that encapsulation involves mass transport from the oxide support onto the surface of metal particles, leading to the formation of a suboxide and the SMSI state. Various reaction mechanisms were proposed to explain the encapsulation phenomena. For example, Taglauer and Knözinger[17,18] correlated the SMSI state with the surface energy (γ) of the oxide supports. These authors pointed out that oxides with low surface energy, for example, TiO_2 and V_2O_5, more easily undergo the SMSI state than oxides with relatively high surface energies, such as SiO_2 and Al_2O_3. The studies and interpretations of Gao et al.[13] lead to a big progress in understanding encapsulation reactions. These authors discussed the effect of the metal's surface energy, suggesting that metals with high surface energy (e.g., Pt and Pd, but not Au, Cu) favor encapsulation. It was proposed that minimization of surface energy is one of the main driving forces for encapsulation.[13,17,18] Another important point is the effect of subsurface nonstoichiometry of TiO_2 on encapsulation reactions of Pt and Rh on TiO_2, which was also studied in great detail.[13,14] From these experiments, it was concluded that the decoration of clusters mainly depends on the existence of oxygen vacancies in the TiO_2 which were introduced by reduction or sputtering. In addition, the balance between the metal−metal bonding and metal−oxide bonding has also been ascribed to the thermodynamic driving force of the decoration.[12,15] One main message of these studies is that surface and interface energies and the oxide's defect structure are major parameters affecting the encapsulation processes.

In the present study, we will work out the influence of the oxide's electronic structure on the encapsulation process and show how a modification of the interfacial electronic structure allows one to control this process. For this purpose, we studied interfacial reactions between Pd clusters and single-crystal TiO_2

* Corresponding author. Tel.: +49-711−689 1429. Fax: +49-711-689 1472. E-mail: t.wagner@fkf.mpg.de.

10.1021/jp046091u CCC: $30.25
Published on Web 12/08/2004

TABLE 1: Treatment Conditions for the Six TiO_2 Crystals[a]

crystals	surface preparation	color − *n*	encapsulation
#A, undoped	standard procedure	pale gray − low	no
#B, undoped	standard procedure plus UHV heating at 800 °C for 9 h	blue − high	yes
#C, doped	standard procedure	dark blue − high	yes
#D, doped	standard procedure plus UHV heating at800 °C for 9 h	dark blue − high	yes
#E, undoped	standard procedure plus light sputtering (200 eV, 1 min)	pale gray − low	no
#F, undoped	standard procedure plus heavy sputtering (1000 eV, 10 min)	light blue − high	yes

[a] A qualitative evaluation of the electron density (n) in CB of TiO_2 was performed considering the defect chemistry of TiO_2 and the crystal's color after treatment.

(110) via XPS, AES, and Rutherford backscattering spectrometry (RBS). On the basis of our results, we will discuss the strong influence of interfacial space charges on encapsulation reactions and contribute to the basic understanding of the reaction mechanisms of encapsulation at metal/oxide interfaces.

2. Experimental Section

Undoped and Nb-doped (Nb: donor, 0.01 at. %) TiO_2 (110) single crystals were used as substrates. Six fresh TiO_2 crystals were differently treated to vary their electronic structures. All crystals were subjected to Ar^+ sputtering (200 eV, 10 min) followed by UHV annealing (800 °C, 1 h) to obtain clean surfaces and to avoid any charging effects during surface measurements. Four of the six crystals were subjected to further treatments (see details in Table 1). After the treatments, AES and XPS measurements failed to detect any surface contaminants. Subsequently, Pd clusters (nominal thickness $\approx$ 1.5 nm) were grown on the differently treated TiO_2 surfaces at 200 °C. Pd was evaporated from an effusion cell with a high-purity alumina crucible at a rate of 0.1 Å/s in a multichamber molecular-beam epitaxy (MBE) system (Metal 600, DCA Instrument).[19] The Pd clusters were stepwise annealed for 30 min at temperatures ranging from 200 to 720 °C. Heating was performed using a BN resistance heater. The temperature of the samples was measured via a calibrated W-Re thermocouple. Following every annealing step, AES and XPS measurements were conducted at room temperature to gain information about the interfacial chemical composition and bonding.

We performed XPS measurements with a Mg Kα X-ray source (E = 1253.6 eV, 400 W) and a double-pass cylinder mirror analyzer (DPCMA) (Perkin-Elmer, 15-255G, $\Delta E/E$ = 0.5%) at a pass energy of 50 eV. During XPS measurements, we did not observe any charging of the TiO_2 crystals. The $Ti2p_{3/2}$ peak at 459.15 eV was used as the reference binding energy (BE) for all core levels. We recorded all AES spectra with the same DPCMA at a constant flux of 20 μA of primary electrons and a primary energy of 3 keV. The Auger electrons were recorded in the direct $EN(E)$ mode, and the spectra were differentiated to obtain the Auger peak-to-peak heights (APPH).[20]

The thicknesses of the titania overlayers of the encapsulated Pd clusters were measured by high depth resolution RBS. To obtain the required energy resolution, the electrostatic spectrometer at the Pelletron of the Max Planck Institute of Metals Research in Stuttgart was used.[21,22] It provides energy resolutions in the 10^{-3} range and in this way allows monolayer depth resolution.[22] In the present case, backscattering of 1 MeV He ions by the Pd clusters was registered at an angle of 75° and symmetric incidence and exit conditions of the ion beam. To improve the depth resolution of the set up, in some cases grazing incidence was used, that is, angles of ion incidence and exit of 5° and 70°, respectively.

3. Results and Discussion

3.1. Defect and Electronic Structure of TiO_2. The defect chemistry and electronic structure of solid-state TiO_2 materials have been studied extensively (see ref 23 and references therein). It is well accepted that the main ionic defects in TiO_2 are interstitial titanium ions ($Ti_i^{\bullet\bullet\bullet\bullet}$ or $Ti_i^{\bullet\bullet\bullet}$) and oxygen vacancies ($V_O^{\bullet\bullet}$ or $V_O^{\bullet}$) (Kröger−Vink notation). The transport of Ti and O in TiO_2 can be described by the interstitial and vacancy models, respectively.[23−26] The concentration of the intrinsic ionic defects as well as the electronic defects (electrons and holes) is a function of temperature, gas pressure, dopant concentration, annealing time, etc. The electronic structure of TiO_2 can be sensitively modified in different ways.[27−31]

The HTR of TiO_2 in UHV or other reducing atmospheres, for example, H_2, leads to the formation of Ti or O defects, for example, oxygen vacancies, acting as intrinsic donors. These treatments modify the electronic structure of the material. Stoichiometric rutile TiO_2 is an insulator with a band gap of 3.05 eV at room temperature. For the nonstoichiometric TiO_{2-x} after reduction, defect states (essentially Ti^{3+}) are present in the band gap at $\geq$2.3 eV above the valence band maximum.[28] If the density of the defect sates is sufficiently high, they can develop into a shallow conduction band, producing free electrons in the conduction band (CB) and thereby shifting the Fermi level (E_F) toward the CB edge.[27,28] All of our crystals were subjected to a rather short HTR in UHV (800 °C, 1 h). The as-received undoped crystals are transparent, with a pale yellow color. This HTR resulted only in a weak color change from pale yellow to pale gray (#A). In contrast, a blue color of the crystals (#B) was observed after fairly long HTR treatments (800 °C, 10 h). The intensity of this blue color corresponds to variations of the electrical conductivity and thus different electron density in the conduction band of TiO_2.[25,26] A darker color of the TiO_2 crystals (long time HTR, #B) corresponds to a higher electron density. Because the oxygen exchange reaction at TiO_2 surfaces is a kinetic limiting process, it can be understood that a high electron density in the CB and strong n-type doping of TiO_2 can only be obtained after long time reduction (10 h in our work).

Routinely, doping is used to change the conductivity in oxides.[32] It is known that Nb-doping in the parts-per-thousand range gives rise to the formation of shallow donor states 0.02−0.03 eV below the conduction band minimum, like the states introduced by oxygen vacancies, causing n-type semiconducting of TiO_2.[29−31] The as-received Nb-doped (Nb, 0.01 at. %) crystal is dark blue, suggesting that the electron density in the CB is quite high even without long time HTR treatment (#C).

Crystal #D was Nb-doped (like #C) and subjected to long HTR treatment like #B. Thus, the electron density in #D is even higher than those of #B and #C.

In addition, Ar^+ sputtering preferentially removes O atoms from the surface or near-surface regions, resulting in an increase of oxygen vacancies in the TiO_2.[27,28] As expected, sputtering changes the surface electronic structure. In the case of crystal #E, a low-energy and brief Ar^+ bombardment (200 eV, 1 min) mainly changes the electronic structure of the top surface layer. In contrast, a high-energy and extended Ar^+ sputtering, as in the case of crystal (#F), leads to a strong reduction of subsurface regions in TiO_2.[14]

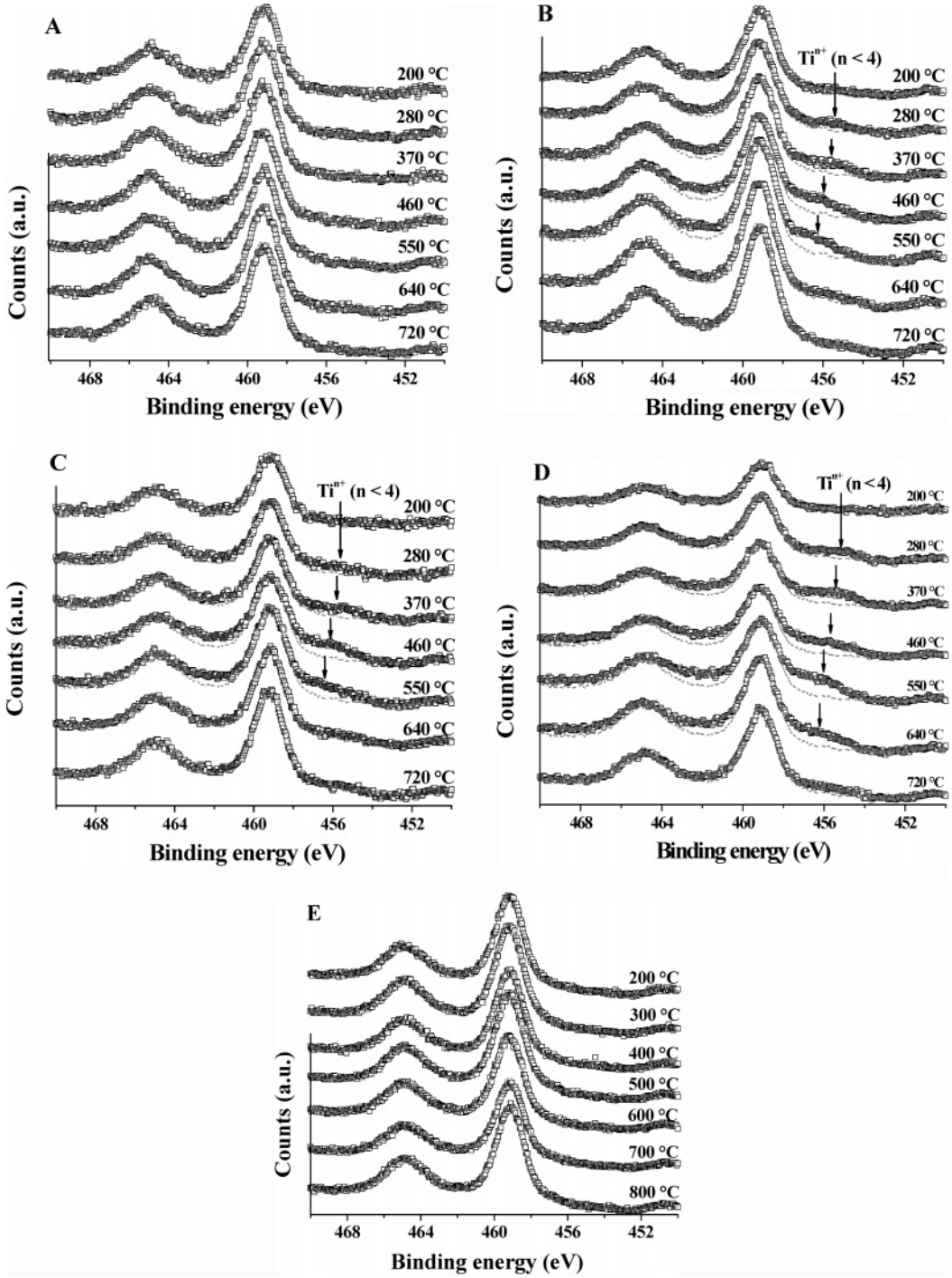

Figure 1. (A−D) Ti2p XPS spectra of differently treated TiO_2 (110) crystals covered with around 1.5 nm (nominal thickness) of Pd after annealing at different temperatures in UHV. (A) Undoped TiO_2 (#A); (B) reduced TiO_2 (#B); (C) doped TiO_2 (#C); (D) reduced and doped TiO_2 (#D); (E) Ti2p spectra from uncovered TiO_2 (#C) (without Pd clusters) annealed at different temperatures in UHV. Dotted lines: Ti2p spectrum from a clean and stoichiometric (no shoulder peaks) TiO_2 (110) surface. Arrows mark the positions of the shoulder peaks corresponding to reduced titania (Ti^{n+}, $n < 4$).

Table 1 summarizes the treatment conditions for all TiO_2 (110) crystals. From the color and treatment conditions, we determined the sequence of the electron density in the CB (n) of the six crystals as follows: n (#B, #C, #D, #F) > n (#A, #E). This sequence will be used later to discuss the encapsulation behavior of Pd clusters on the differently treated crystals.

3.2. Thermal Stability of Pd/TiO_2 Interfaces. Our XPS and AES results revealed a strong dependence of the thermal stability of the Pd/TiO_2 interfaces on the different treatment of the TiO_2 crystals. Figure 1 shows a series of Ti2p spectra from the Pd/#A, Pd/#B, Pd/#C, and Pd/#D interfaces, and from a bare crystal annealed at different temperatures. For #A, we failed to detect any changes in the shape of the spectra during annealing (Figure 1A). In contrast, shoulder peaks were clearly observed in the Ti2p spectra from #B, #C, and #D (Figure 1B−D). These additional peaks started to appear at about 280 °C and had their maximum intensity at ∼500 °C. At higher temperatures, for example, 720 °C, virtually symmetric double peaks were again present in the spectra. The shoulder peaks were located between 455.8 and 456.7 eV, indicating the formation of reduced Ti states, (Ti^{n+}, $n < 4$). Increasing the annealing temperature from 280 to 550 °C shifted the peaks to higher binding energies

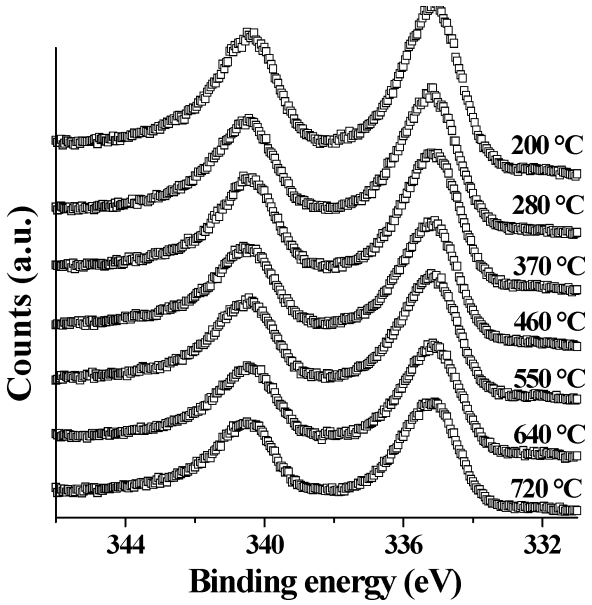

Figure 2. Pd3d XPS spectra of Pd clusters supported on doped TiO_2 (#C) annealed at different temperatures.

(compare arrows in Figure 1B−D). The peak position can be used to determine the chemical states of Ti. It has been shown that the binding energy difference (ΔE) between Ti^{2+} and Ti^{4+} is about 3 eV, while ΔE between Ti^{3+} and Ti^{4+} is around 2 eV.[33] Thus, at 280 °C, the reduced states should mainly originate from Ti^{2+} ($\Delta E \cong 3.3$ eV), whereas at ∼550 °C a mixture of Ti^{2+} and Ti^{3+} states was observed ($\Delta E \cong 2.5$ eV). At temperatures above 640 °C, we observed only the valence state Ti^{4+}.

Figure 1E shows Ti2p spectra from the clean surface of a doped TiO_2 crystal (#C), which was annealed in UHV at different temperatures. For this bare crystal, we did not observe any shoulder peak in the Ti2p spectra, indicating that the appearance of additional peaks in Figure 1B−D is closely related to the Pd−TiO_2 interaction. It is also worth mentioning that no Pd3d spectra showed any changes in the peak positions and peak shapes during annealing. Because the oxidation of Pd results in a BE shift of Pd3d > 1 eV[34] and the formation of a Pd alloy containing Ti, for example, Pd_3Ti, leads to a BE shift of ∼0.5 eV,[35] the unchanged Pd3d spectra in all temperature ranges indicate chemical inertness of the Pd clusters against oxidation or alloy formation. An example of a set of Pd3d spectra from Pd supported on #C is shown in Figure 2.

The formation of Ti^{n+} ($n < 4$) species at metal/TiO_2 interfaces may originate from two interactions:[36,37] (i) a redox reaction, that is, oxidation of the metal overlayer and a reduction of TiO_2, and (ii) encapsulation. Redox reactions will lead to the oxidation of the metal overlayers and, in addition, the formation of Ti^{n+} ($n < 4$) (reduction of the oxide substrate). As expected, we did not observe oxidation of Pd (see Figure 2). Therefore, the presence of reduced states detected in the Pd/#B, Pd/ #C, and Pd/#D systems originated from encapsulation of Pd by reduced titania (TiO_x, $x < 2$).

Figure 3 shows the ratio of the APPH of the O (503 eV) to Ti (418 eV) signal. This ratio decreased for the Pd/#B, Pd/#C, and Pd/#D samples with increasing temperature, finally passing through a shallow minimum at about 450 °C. With further increasing temperature, the O/Ti ratio increased. In contrast, the O/Ti ratio stayed virtually constant for the Pd/#A sample and an uncovered TiO_2 crystal annealed under identical conditions. Such a change of Auger O/Ti ratios has been attributed

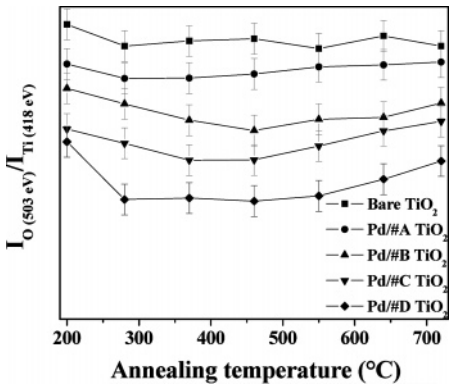

Figure 3. Ratios of Auger O (503 eV) and Ti (418 eV) signals from (A) bare TiO_2 (110) surface, (B) Pd/undoped TiO_2 (#A), (C) Pd/reduced TiO_2 (#B), (D) Pd/doped TiO_2 (#C), and (E) Pd/reduced and doped TiO_2 (#D) subjected to stepwise annealing in UHV.

to reconstructions of TiO_2 (110) surfaces caused by UHV annealing.[38,39] However, our AES measurements on uncovered bare crystal surfaces indicated that we can neglect the influence of reconstructions. The decrease of the O/Ti ratio at relatively low temperatures suggests an enrichment of the surfaces with Ti; at temperatures above 450 °C, this enrichment decreases. The results obtained via AES measurements are quite consistent with those obtained by XPS, demonstrating quite a weak interaction between Pd and crystal #A. For crystals #B, #C, and #D, however, the interaction between Pd and substrate resulted in an encapsulation of Pd clusters by a reduced titania overlayer.

As stated in section 2, the thicknesses of the titania overlayers of the encapsulated Pd clusters were determined by high-resolution RBS. Figure 4 shows (A) the RBS spectra of the Pd clusters for symmetric scattering conditions, that is, 37.5° ion incidence and 37.5° exit angle. The peaklike structures seen directly provide the thickness distributions of the Pd clusters: while samples #A−#C are similar, #D is relatively thicker. The peak areas yield the mean nominal thicknesses of the Pd layers which amount to #A, 1.0 nm; #B, 1.5 nm; #C, 1.4 nm; and #D, 2.5 nm. From the relative peak heights (relative to the RBS spectrum of a solid Pd sample, see figure) the coverage of the substrate is derived which amounts to #A, 0.38; #B, 0.42; #C, 0.35; and #D, 0.62.

The thicknesses of the titania cover layers above the encapsulated Pd clusters were determined from the energy shifts of the high-energy edges of the RBS spectra of the covered clusters with respect to the edges of the uncovered clusters #A. As is evident from Figure 4A, it is no simple task to derive any energy shift from the spectra of this figure. Therefore, and to further improve the depth resolution of the technique, grazing incidence of the ion beam (5° from the surface) was used (Figure 4B). Under these conditions, all spectra exhibit (at least short) plateaus of the same height at the high energy end of the spectra, which allow a simple determination of the energy shifts. With respect to the spectrum of the uncovered sample #A, the shifts amount to #B, 0.78 keV; #C, 0.88 keV; and #D, 1.67 keV. With the assumption of a stoichiometric composition TiO_2 of these layers, one obtains thicknesses of #B, 0.13 nm; #C, 0.14 nm; and #D, 0.27 nm.

The interaction between Pd clusters and sputtered TiO_2 crystals, #E and #F, was also studied by UHV annealing and XPS measurement. Ar^+ bombardment produces Ti^{n+} ($n < 4$) species at the TiO_2 surface, causing shoulder peaks at low binding energies in the Ti2p spectra. Such reduced states can be completely removed by annealing the surface in UHV. Figure

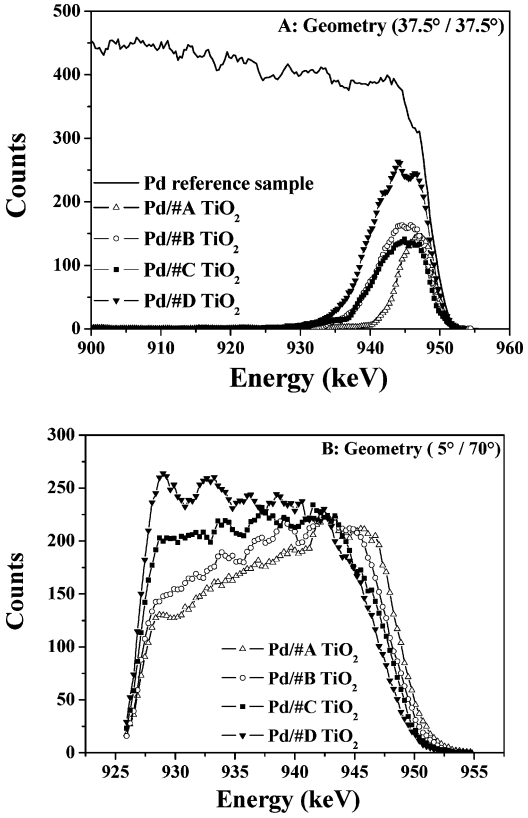

Figure 4. (A) RBS spectra of UHV annealed Pd supported on TiO_2 from samples #A to #D and symmetric scattering conditions (angle of ion incidence to surface = exit angle = 37.5°). For comparison, the spectrum of solid Pd is shown (full line). The nominal layer thicknesses are obtained from the peak areas, and from the peak heights the coverages are obtained. (B) Same as (A) but for incidence and exit angles of 5° and 70°, respectively. A shift of the high-energy edges of the RBS spectra for samples #A−#D is clearly visible and is caused by an increasing encapsulation with titania.

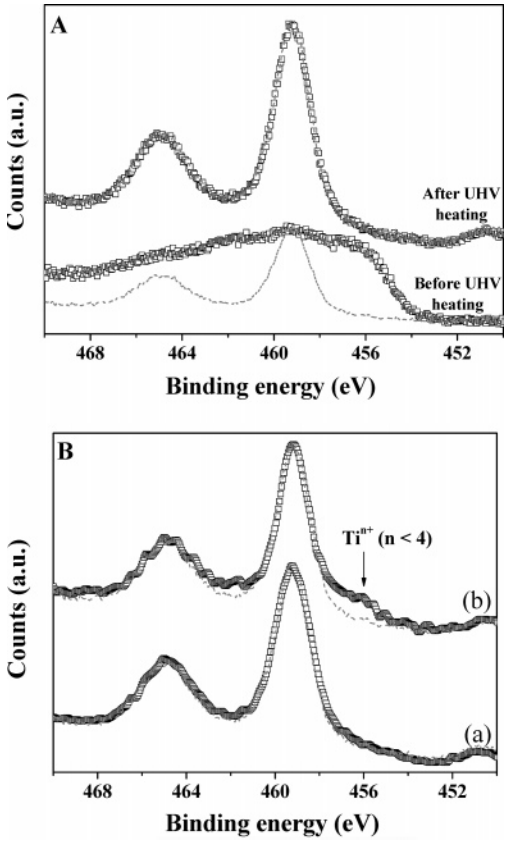

Figure 5. (A) Ti2p spectra of the TiO_2 (110) surface, strongly sputtered by Ar^+ before and after UHV annealing at 550 °C for 0.5 h. (B) Ti2p spectra of the TiO_2 (110) surfaces: (a) after light Ar^+ sputtering (#E) and (b) after strong Ar^+ sputtering (#F) covered with Pd and then subjected to UHV annealing at 550 °C for 0.5 h. Dotted lines: Ti2p spectrum from a clean and stoichiometric (no shoulder peaks) TiO_2 (110) surface. An arrow marks the position of the shoulder peak corresponding to reduced titania (Ti^{n+}, $n < 4$).

5A shows the Ti2p spectra of a strongly sputtered TiO_2 surface (1000 eV, 10 min, #F) before and after UHV annealing. The double peaks in the spectrum become virtually symmetric after UHV annealing at 550 °C for 0.5 h. However, the evolution of the Ti2p spectra during UHV annealing (550 °C, 0.5 h) was different if the sputtered surfaces were coated with Pd clusters (Figure 5B). In this case, a shoulder peak can still be seen in the Ti2p spectrum. In contrast, such a shoulder peak was not observed for Pd supported on a lightly sputtered crystal (#E) (Figure 5B). Comparing the results shown in Figure 5A and B allows one to conclude that encapsulation occurred in the system Pd/#F, while the Pd clusters in the Pd/#E system were not encapsulated. These results are consistent with those obtained by Berkó et al.[14] for the Rh/TiO_2 (110) system.

The above investigation of the thermal stability of Pd/TiO_2 interfaces reveals that the interaction of Pd clusters with TiO_2 (110) depends strongly on the crystal pretreatment: UHV heating resulted in encapsulation of Pd on crystals #B, #C, #D, and #F, whereas Pd did not experience encapsulation on crystals #A and #E (Table 1). Correlating the encapsulation reaction to the electron density in TiO_2 supports the following conclusion: the encapsulation of Pd on TiO_2 depends mainly on the electron density in the CB of the TiO_2 crystals; strong n-type doped TiO_2 crystals favor encapsulation.

3.3. Basic Mechanisms for Encapsulation of Metal Clusters on Oxide Supports. It has been shown that the encapsulation reactions at metal/TiO_2 interfaces involve the formation of reduced titania TiO_x ($x < 2$) layers which decorate the top of the metal clusters. We suggest that this reaction includes the following steps: (i) the amplified Ti outward diffusion in comparison to O outward diffusion toward the TiO_2 surface (Figure 6A), enabling (ii) the formation of a Ti-rich decoration layer (TiO_x ($x < 2$)) on top of the Pd clusters (Figure 6B).

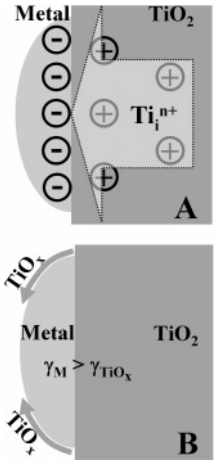

Figure 6. Schematic drawing of the major mass transport processes during encapsulation. (A) Outward diffusion of Ti_i^{n+} in TiO_2 assisted by positive space charges near the interface. (B) Mass migration of TiO_x ($x < 2$) onto metal clusters driven by the minimization of surface energy.

Step (i) (Figure 6A). The first process is dominated by the mass transport of Ti out of the crystal. Considering the defect

chemistry of TiO_2, the process must be balanced by an outward diffusion of interstitial titanium cations, Ti_i^{n+} ($n = 3$ or 4), in the TiO_2 near-surface region. This diffusion is driven by the difference in the electrochemical potential of Ti_i^{n+} across the phase boundary. It is well established that Ti interstitials possess a high diffusivity in TiO_2 at elevated temperatures (e.g., 500−800 K). The vertical diffusion of Ti_i^{n+} between the surface and the bulk was regarded as the dominant process for two important TiO_2 surface reactions: the reoxidation of Ar^+ sputtered surfaces by vacuum annealing,[40,41] and the effect of oxygen-induced surface restructuring.[11,42−44] The diffusion direction for these reactions is quite different. In the former process, Ti_i^{n+} diffuses to the bulk, while the latter one necessitates the transport of Ti_i^{n+} from the bulk to the surface. We propose that the Ti ion diffusion in TiO_2 at relatively low temperatures is kinetically limited and, therefore, strongly coupled with space charges at the surfaces. For the Ar^+ sputtered TiO_2, surface oxygen vacancies create defect states and donate electrons to the system. The bands of TiO_2 bend downward, leaving positive charges on the surface and an accumulation of electrons in the near-surface region (see Figure 1 in ref 15 and Figure 35 in ref 23). The surface positive charges drive the inward diffusion of Ti_i^{n+} for the reoxidation of sputtered surfaces by vacuum heating (the reverse case of that shown in Figure 6A). Exposure of the reduced TiO_2 surfaces to O_2 at room temperature gives rise to the unbending of the bands due to annihilation of the surface oxygen vacancies.[23,28] Furthermore, the large electronegativity of O_2, that is, the low electronic energy level of the molecule, enables the acceptance of electrons from TiO_2 and results in the upward bending of the TiO_2 bands. Negative charges on TiO_2 surfaces (essentially O^{2-}) extract the Ti_i^{n+} diffusion from the bulk to the surface where they react with oxygen to form TiO_2 on the surface (Figure 6A).

Like the oxygen-induced surface restructuring reaction, the outward diffusion of Ti_i^{n+} of the encapsulation reaction also needs to be extracted by the charges distributed as shown in Figure 6A. This requires that the work function (ϕ) of the metal must be larger than that of TiO_2 (ϕ (metal) > ϕ (TiO_2)); in other words, for a metal with large ϕ and strong n-type doped TiO_2, E_F (TiO_2) > E_F (metal). After the vacuum levels of two materials are aligned (contact of the materials), E_F of the metal will be below the donor states-induced shallow conduction band of TiO_2. The equilibration of both E_F results in a charge transfer from the occupied donor states in TiO_2 to the metal and an upward bending of the TiO_2 bands, forming negatively charged metal clusters on the surface and positive space charges in TiO_2 (Figure 6A). We would like to mention here that this process is similar to the Schottky-type contact between metals and semiconductors.[6,45] On the basis of the above considerations, we suggest that the reaction kinetics of encapsulation is mainly controlled by the electronic structure of the metal and the TiO_2. Encapsulation is possible for contacts between n-type doped TiO_2 and metals with large work functions, such as Pd ($\phi_{Pd(111)} \approx 5.6$ eV[46]) and TiO_2 #B, #C, #D, and # F ($\phi_{TiO_2(110)} \approx 5.2$ eV[27,47]) in our work. However, the density of defect states in TiO_2 #A and #E may not be sufficiently high to allow the presence of delocalized electrons in the CB and strong n-type doping. In this case, there will be no or only a very weak charge transfer from the TiO_2 #A and #E to the Pd after establishing contact. Thus, Ti_i^{n+} cannot be extracted to surfaces.

Step (ii) (Figure 6B). The second process involves mass transport of TiO_x ($x < 2$) onto the surface of the metal clusters. Recently, this transport process was assigned to mass migration along the surface of the metal clusters (Figure 6B).[48] As discussed by Taglauer and Knözinger,[17,18] the wetting of metal clusters by reduced oxide layers is influenced by the surface energies of the metal and the oxide. This means that encapsulation is also driven thermodynamically by a minimization of the surface energies of the system. Encapsulation is possible in the case of low surface energies of the oxides (γ_{TiO_x}) and high surface energies of the metals (γ_M), that is, $\gamma_{TiO_x} < \gamma_M$.[13,18]

In conclusion, the encapsulation reaction at metal/TiO_2 interfaces requires TiO_2 crystals with high electron density or strong n-type doping (Table 1), as well as metals with large work functions and high surface energies, for example, Pd. The reaction process at the interface can be described as follows. The contact between the oxide and the metal will establish positive space charges in TiO_2 (see Figure 6A). They drive the outward diffusion of Ti_i^{n+} but hinder the outward diffusion of oxygen anions (O^{2-}) at relatively low temperatures. Such a difference in the diffusion rates of Ti and O enables the enrichment of Ti at the surface ($T < 450$ °C in Figure 3). On the other hand, the outward diffusion of Ti_i^{n+} will gradually weaken the positive space charges, which allows the outward diffusion of oxygen anions, thus favoring the formation of TiO_x ($x < 2$) on the surface (see Figure 1B−D). Due to the difference of the surface energy of the TiO_x and the metal, TiO_x tends to cover the surface of the metal clusters, resulting in encapsulation. At high temperatures, the O outward diffusion will be thermally activated. Thus, an increase in annealing temperature changes the decorating layers from Ti-rich to a more stoichiometric TiO_2 (Figure 1 and $T > 450$ °C in Figure 3). At the same time, the chemical state of Ti changes gradually from Ti^{2+} to Ti^{4+} (see Figure 1B−D). This indicates why several groups have observed differences in the chemical compositions of the TiO_x encapsulating layers.[9,10,14,17]

More generally, other oxides, such as CeO_2 and La_2O_3, may experience encapsulation as TiO_2.[8,49] These oxides were treated under quite different conditions to induce encapsulation reactions, such as HTR in H_2,[1−4,7,8] HTR in UHV,[9−17,49] sputtering reduction of the oxide,[14] oxide doping via extrinsic donors (present work), etc. A common feature of all of these treatments and processes is that they will induce n-type doping of oxides and the formation of mobile ionic defects in the oxides. Some oxides such as SnO_2 can also be reduced by vacuum heating. However, the large work function or large electron affinity of the oxides[27] may lead to ϕ (metal) < ϕ (oxide), and encapsulation cannot occur. Even under extreme conditions, the electronic structure and defect chemistry of stable oxides (SiO_2, Al_2O_3, etc.) cannot be modified in such a manner that SMSI reactions are possible. Concerning the metals, a variety of studies revealed that Pt, Pd, Rh, Ni, and Ir were subjected to encapsulation.[7−18,23,50,51] Obviously, this behavior is favored by a large work function of the metals, for example, $\phi_{Pt(111)} = 5.93$ eV,[46] $\phi_{Pd(111)} = 5.6$ eV,[46] and $\phi_{Rh(111)} = 5.3−5.6$ eV,[52,53] as well as sufficiently high surface energies ($\gamma > 2$ J m^{-2})[54−56] (region I in Figure 7). The transition metals, for example, Cu, Ag, Au, and Co, possess either small work functions or low surface energies. These metals are well known to withstand encapsulation.[23] The above-discussed results are quite consistent with the mechanisms discussed in steps (i) and (ii).

In the case of encapsulation, $E_{F(oxide)} > E_{F(metal)}$ (see step (i)) results in an upward band bending, which was confirmed by different authors via surface photoemission investigations or the measurement of the Schottky barrier height of metal/oxide junctions.[14,15,47,57] For example, upward bending of 0.8 eV was observed upon 1 ML Rh adsorption onto reduced TiO_2 (110) by Henrich and co-worker.[15] A depletion layer in TiO_2 and a

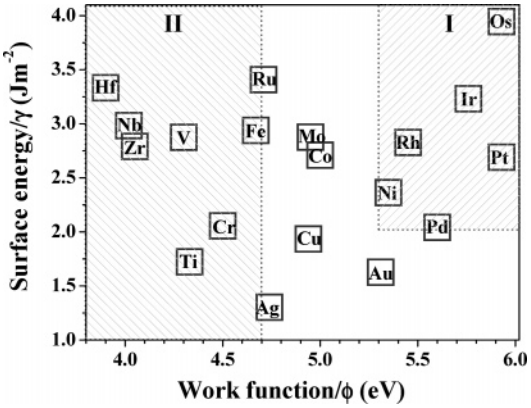

Figure 7. Relationship between surface energy γ_M and work function ϕ of different transition metals. If available, for fcc metals values of the (111) surfaces and for bcc metals values of (100) surfaces are displayed because of the orientation of the metals on TiO_2 (110).[23] For all other metals, values of ϕ are taken from polycrystalline samples.[46] The surface energy data were taken from calculations of Mezey and Giber;[54] these data are qualitatively consistent with experimental data,[55,56] providing larger γ values for Pt, Pd, Rh, and Ir and smaller γ values for Au, Ag, and Cu. In region I, encapsulation is expected ($\phi >$ 5.3 eV and $\gamma > 2$ Jm^{-2}); in region II ($\phi <$ 4.7 eV), oxidation of metals on TiO_2 is possible.[58]

band bending of −0.9 eV was observed at Pt/TiO_2 (110) diodes by Schiebaum et al. (ref 47 and references therein). In agreement with that, our XPS measurements also showed a negative BE shift of the TiO_2 core levels ($\sim$ −0.3 eV) due to upward band bending after Pd deposition. In contrast, metals with a small work function, such as alkali metals and early transition metals, are instead oxidized on oxides like TiO_2, $SrTiO_3$, etc. (see region II in Figure 7).[23,36,37] The adsorption of these metals stimulates the outward diffusion of oxygen anions across the interface by negative space charges at the interfaces formed by a transfer of electrons from the metal to the oxide in the case of $E_{F(oxide)} < E_{F(metal)}$.[58]

We should point out that the SMSI at metal/oxide interfaces is quite complicated. The occurrence of encapsulation reactions is sensitively influenced by many factors. For example, our present work shows that slight Nb doping promotes such a reaction. However, high level Nb doping in TiO_2 does not contribute to free electrons in the CB but stabilizes the surface by forming Nb−O bonds, which suppresses SMSI for Pt on TiO_2.[13] Relatively high temperatures are necessary to activate the diffusion of Ti ions in TiO_2 and enable diffusion of TiO_x species ($T > T_{Hüttig}$),[18] while too high temperatures caused the formation of metal alloys or metal solid solutions.[8] The reaction is also strongly influenced by the history of the oxide crystals (pretreatment), the size of metal clusters, the crystallographic orientation of the oxide surfaces, etc. This may explain that encapsulation reactions were observed only by some research groups, although other groups applied very similar conditions to the same metal/oxide system (e.g., refs 12, 13 versus 57 in Pt/TiO_2, and refs 10 versus 59 in Pd/TiO_2). While further comprehensive studies are needed to understand the strong interaction at metal/oxide interfaces in more detail, our research may provide some clue for more sophisticated investigation.

4. Conclusion

In the Pd/TiO_2 systems, it can be concluded that the encapsulation reaction depends on the electronic structure of TiO_2. Strong n-type doping of TiO_2 favors encapsulation. This reaction process depends on the amplified outward diffusion of Ti_i^{n+} toward the TiO_2 surfaces and the migration of TiO_x onto the surface of the metal clusters. The preferential outward diffusion of Ti cations requires E_F (TiO_2) > E_F (metal), and encapsulation of metal clusters by TiO_x layers is favored by the relatively high surface energies of the metals. These requirements can be used to understand encapsulation reactions for other metal/oxide systems. Accordingly, it can be concluded that the following prerequisites are necessary for encapsulation of metal clusters on oxide supports: (1) E_F (oxide) > E_F (metal); (2) reduced or n-type doped oxides with small surface energies, such as TiO_2, CeO_2; (3) metals with large work functions and large surface energies, for example, Pt, Pd, Rh, Ni, Ir, and maybe Os (Figure 7); and (4) sufficiently high temperatures to activate transport processes. Such mechanisms enable us to control the encapsulation reaction or SMSI in many metal/oxide catalytic systems.

Acknowledgment. We gratefully acknowledge valuable discussions with C. Elsässer, J. Fleig, J. Howe, R. Merkle, and M. Rühle.

References and Notes

(1) Schwab, G. M. *Adv. Catal.* **1978**, *27*, 1.
(2) Tauster, S. J.; Fung, S. C.; Garten, R. L. *J. Am. Chem. Soc.* **1978**, *100*, 170.
(3) Tauster, S. J.; Fung, S. C.; Baker, R. T. K.; Horsley, J. A. *Science* **1981**, *211*, 1121.
(4) Haller, G. L.; Resasco, D. E. *Adv. Catal.* **1989**, *36*, 173.
(5) Vayenas, C. G.; Brosda, S.; Pliangos, C. *J. Catal.* **2003**, *216*, 487.
(6) Ioannides, T.; Verykios, X. E. *J. Catal.* **1996**, *161*, 560.
(7) Bernal, S.; Botana, F. J.; Calvino, J. J.; López, C.; Pérez-Omil, J. A.; Rodríguez-Izquierdo, J. M. *J. Chem. Soc., Faraday Trans.* **1996**, *92*, 2799.
(8) Bernal, S.; Calvino, J. J.; Cauqui, M. A.; Gatica, J. M.; López Cartes, C.; Pérez-Omil, J. A.; Pintado, J. M. *Catal. Today* **2003**, *77*, 385.
(9) Dulub, O.; Hebenstreit, W.; Diebold, U. *Phys. Rev. Lett.* **2000**, *84*, 3646.
(10) Bennett, R. A.; Pang, C. L.; Perkins, N.; Smith, R. D.; Morrall, P.; Kvon, R. I.; Bowker, M. *J. Phys. Chem. B* **2002**, *106*, 4688.
(11) Bennett, R. A.; Stone, P.; Bowker, M. *Catal. Lett.* **1999**, *59*, 99.
(12) Pesty, F.; Steinrück, H. P.; Madey, T. E. *Surf. Sci.* **1995**, *339*, 83.
(13) Gao, Y.; Liang, Y.; Chambers, S. A. *Surf. Sci.* **1996**, *365*, 638.
(14) Berkó, A.; Ulrych, I.; Prince, K. C. *J. Phys. Chem. B* **1998**, *102*, 3379.
(15) Sadeghi, H. R.; Henrich, V. E. *J. Catal.* **1988**, *109*, 1.
(16) Sadeghi, H. R.; Henrich, V. E. *Appl. Surf. Sci.* **1984**, *19*, 330.
(17) Labich, S.; Taglauer, E.; Knözinger, H. *Top. Catal.* **2001**, *14*, 153.
(18) Knözinger, H.; Taglauer, E. In *Handbook of Heterogeneous Catalysis*; Ertl, G., Knözinger, H., Weitkamp, J., Eds.; VCH: Weinheim, 1997; p 216.
(19) Wagner, T.; Richter, G.; Rühle, M. *J. Appl. Phys.* **2001**, *89*, 2606.
(20) Fu, Q.; Wagner, T. *Phys. Rev. Lett.* **2003**, *90*, 106105.
(21) Enders, Th.; Rilli, M.; Carstanjen, H. D. *Nucl. Instr. Methods Phys. Res., Sect. B* **1992**, *64*, 817.
(22) Carstanjen, H. D. *Nucl. Instr. Methods Phys. Res., Sect. B* **1998**, *136−138*, 1183.
(23) Diebold, U. *Surf. Sci. Rep.* **2003**, *48*, 53.
(24) Sasaki, J.; Peterson, N. L.; Hoshino, K. *J. Phys. Chem. Solids* **1985**, *46*, 1267.
(25) Li, M.; Hebenstreit, W.; Diebold, U.; Tyryshkin, A. M.; Boeman, M. K.; Dunham, G.; Henderson, M. A. *J. Phys. Chem. B* **2000**, *104*, 4944.
(26) Sekiya, T.; Yagisawa, T.; Kamiya, N.; Das Mulmi, D.; Kurita, S.; Murakami, Y.; Kodaira, T. *J. Phys. Soc. Jpn.* **2004**, *73*, 703.
(27) Henrich, V. E.; Cox, P. A. *The Surface Science of Metal Oxides*; Cambridge University Press: Cambridge, 1994.
(28) Henrich, V. E.; Dresselhaus, G.; Zeiger, H. J. *Phys. Rev. Lett.* **1976**, *36*, 1335.
(29) Batzill, M.; Katsiev, K.; Gaspar, D. J.; Diebold, U. *Phys. Rev. B* **2002**, *66*, 235401.
(30) Morris, D.; Dou, Y.; Rebane, J.; Mitchell, C. E. J.; Egdell, R. G.; Law, D. S.; Vittadini, A.; Casarin, M. *Phys. Rev. B* **2000**, *61*, 13445.
(31) Chambers, S. A.; Gao, Y.; Kim, Y. J.; Henderson, M. A.; Thevuthasan, S.; Wen, S.; Merkle, K. L. *Surf. Sci.* **1996**, *365*, 625.
(32) Smyth, D. M. *Solid State Ionics* **2000**, *129*, 5.
(33) Mayer, J. T.; Diebold, U.; Madey, T. E.; Garfunkel, E. *J. Electron Spectrosc. Relat. Phenom.* **1995**, *73*, 1.

(34) Moulder, J.; Stickle, W. F.; Sobol, P. E.; Bomben, K. D. *The Handbook of the X-ray Photoelectron Spectroscopy*; Perkin-Elmer Corp.: 1992.

(35) Hillebrecht, F. U.; Fuggle, J. C.; Bennett, P. A.; Zolnierek, Z.; Feiburg, Ch. *Phys. Rev. B* **1983**, *27*, 2179.

(36) Diebold, U.; Pan, J. M.; Madey, T. E. *Surf. Sci.* **1995**, *331−333*, 845.

(37) Campbell, C. T. *Surf. Sci. Rep.* **1997**, *27*, 1.

(38) Stone, P.; Bennett, R. A.; Poulston, S.; Bowker, M. *Surf. Sci.* **1999**, *433−435*, 501.

(39) Xu, C.; Lai, X.; Zajac, G. W.; Goodman, D. W. *Phys. Rev. B* **1997**, *56*, 13464.

(40) Henderson, M. A. *Surf. Sci.* **1995**, *343*, L1156.

(41) Henderson, M. A. *Surf. Sci.* **1999**, *419*, 174.

(42) Onishi, H.; Iwasawa, Y. *Phys. Rev. Lett.* **1996**, *76*, 791.

(43) Bennett, R. A.; Stone, P.; Price, N. J.; Bowker, M. *Phys. Rev. Lett.* **1999**, *82*, 3831.

(44) Li, M.; Hebenstreit, W.; Gross, L.; Diebold, U.; Henderson, M. A.; Jennison, D. R.; Schultz, P. A.; Sears, M. P. *Surf. Sci.* **1999**, *437*, 173.

(45) Sze, S. M. *Physics of Semiconductor Devices*; John Wiley & Sons: New York, 1981.

(46) Weast, R. C., Astle, M. J., Ed. *CRC Handbook of Chemistry and Physics*, 63rd ed.; CRC Press: Boca Raton, FL, 1982.

(47) Schierbaum, K. D.; Fisher, S.; Wincott, P.; Hardman, P.; Dhanak, V.; Jones, G.; Thornton, G. *Surf. Sci.* **1997**, *391*, 196.

(48) Suzuki, T.; Souda, R. *Surf. Sci.* **2000**, *448*, 33.

(49) Mullins, D. R.; Zhang, K. Z. *Surf. Sci.* **2002**, *513*, 163.

(50) Aizawa, M.; Lee, S.; Anderson, S. L. *J. Chem. Phys.* **2002**, *117*, 5001.

(51) Reyes, P.; Aguirre, M. C.; Melián-Cabrera, I.; López Granados, M.; Fierro, J. L. G. *J. Catal.* **2002**, *208*, 229.

(52) Brault, P.; Range, H.; Toennies, J. P.; Wöll, Ch. *Z. Phys. Chem.* **1997**, *198*, 1.

(53) Vanselow, R.; Li, X. Q. D. *Surf. Sci. Lett.* **1992**, *264*, L200.

(54) Mezey, L. Z.; Giber, J. *Jpn. J. Appl. Phys.* **1982**, *21*, 1569.

(55) Tyson, W. R.; Miller, W. A. *Surf. Sci.* **1977**, *62*, 267.

(56) Overbury, S. H.; Bertrand, P. A.; Somorjai, G. A. *Chem. Rev.* **1975**, *75*, 547.

(57) Schierbaum, K. D.; Fischer, S.; Torquemada, M. C.; de Segovia, J. L.; Román, E.; Martín-Gago, J. A. *Surf. Sci.* **1996**, *345*, 261.

(58) Fu, Q.; Wagner, T. *Surf. Sci. Lett.* In press.

(59) Negra, M. D.; Nicolaisen, N. M.; Li, Z.; Møller, P. J. *Surf. Sci.* **2003**, *540*, 117.